Tracer Tests in a Fractured Dolomite

4. Double Porosity, Multiple-Rate Mass Transfer Processes in Two-Well Convergent-Flow Tests

Sean A. McKenna,
Lucy C. Meigs
Sandia National Laboratories,
Geohydrology Department,
PO Box 5800 MS 0735,
Albuquerque, NM 87185-0735
em: samcken@sandia.gov

Roy Haggerty
Department of Geosciences,
104 Wilkinson Hall,
Oregon State University
Corvallis, OR 97331-5506
em: haggertr@ucs.orst.edu

Submitted to Water Resources Research, December, 1998

DISCLAIMER

Abstract

Two-well convergent-flow tracer tests conducted in the Culebra dolomite (Rustler Formation, New Mexico, USA) are analyzed with both single-and multiple-rate, double-porosity models. Parameter estimation is used to determine the mean and standard deviation of a log-normal distribution of diffusion rate coefficients as well as the advective porosity and longitudinal dispersivity. At two different test sites, both multirate and single-rate models are capable of accurately modeling the observed data. Estimated model parameters are tested against breakthrough curves obtained along the same transport pathway at a different pumping rate. Implications of the multirate mass-transfer model at time and length scales greater than those of the tracer tests include the instantaneous saturation of a fraction of the matrix and the possibility of a fraction of the matrix remaining unsaturated at long times.

Introduction

A number of single-well injection-withdrawal (SWIW) and multi-well convergent-flow tracer tests have been conducted in the Culebra dolomite member of the Rustler Formation in the vicinity of the Waste Isolation Pilot Plant (WIPP) in southeastern New Mexico [*Meigs and Beauheim*, this issue]. These tracer tests were conducted with the goal of better characterizing the physical transport parameters of the Culebra dolomite. Modeling of the SWIW test results indicate that matrix diffusion is an important transport process within the Culebra [*Altman et al.*, this issue]. The conceptual model of matrix diffusion within the Culebra was extended from the conventional double-porosity single-rate model to a continuous log-normal distribution of mass-transfer rates [*Haggerty et al.*, this issue]. The multirate diffusion model was shown to provide superior model fits to the observed SWIW test data relative to the conventional single-rate model [*Haggerty et al.*, this issue].

The signature of multirate diffusion processes in a multi-well convergent-flow test is more difficult to discern than in a SWIW test because of added complexity in the physics governing the flow system. Specifically, this added complexity is due to (1) tailing caused by flow-field heterogeneity, a process the SWIW test is designed to mitigate; and (2) the sensitivity of the

tracer transport results to advective porosity. In this paper, we examine the applicability of the multirate diffusion model to a subset of the multi-well convergent-flow tracer tests.

At the H-19 and H-11 hydropads, multiple injection wells were centered around the central pumping well (multiwell testing). In this paper, we examine a single pathway (i.e., one injection well to the pumping well) at each hydropad. As used in this paper, a two-well convergent-flow (TWCF) tracer test is defined as a test with a single injection well and a single withdrawal well having a constant pumping rate. Prior to tracer injection, the pumping rate has been maintained for sufficient time to allow velocities to be considered steady-state within the domain of the tracer test. A slug of tracer is injected into this steady-state convergent-flow system from a second well located a distance, R_∞ away from the pumping well. Immediately following the injection of the tracer, a chaser of Culebra brine (containing no tracer) is injected to flush the injection well of any remaining tracer. At the end of the chaser injection, the injection rate is reduced to zero for the remainder of the tracer test. The discharge at the pumping well remains constant throughout the tracer and chaser injections and throughout the collection of tracer data (up to 50 days).

Tracer tests with two or more wells have been used by a number of researchers to estimate groundwater flow and transport parameters over a volume of aquifer between the injection and recovery wells. As pointed out by *Moench* [1989], a strength of these multiple-well tests is that 100 percent recovery of the injected tracer is theoretically possible thus providing confidence in the conceptual model used to analyze and model the tracer recovery. Numerous tracer tests have been conducted with the goal of determining dispersivity [e.g., *Novakowski et al.,* 1985; *Moench,* 1989; *Welty and Gelhar,* 1994]. Other researchers have used multiwell tracer tests to determine the effective porosity and anisotropy of the flow system [e.g., *Sánchez-Vila and Carrera,* 1997]. Multiwell tracer tests can also provide information on sorption and diffusion processes in fractured rock [*Moench,* 1995; *Haderman and Heer,* 1996;*D'Alessandro et al.,* 1997; *Garcià Gutiérrez et al.,* 1997].

Tracer breakthrough curves (BTC's) in multiwell tests can generally be described as exhibiting a relatively rapid rise to a peak concentration and then a decline in concentration after the peak. The latter portion, or tail, of the BTC may be of the same time-scale as the rise in concentration or considerably longer. The length of the tail is controlled by flow-field

heterogeneity (typically modeled with a dispersivity value) and factors that would retard the transport of solute relative to pure advective flow, such as diffusion into lower velocity zones (e.g., from a fracture to the matrix) or sorption. With this conceptualization, the peak of the BTC in a double porosity system with non-sorbing tracers can be represented by adjusting the advective porosity value, and the tail of the BTC can be represented by adjusting the value of dispersivity and the diffusion coefficient or the effective matrix block size. While the concept of several discrete rates of diffusion has been proposed for modeling transport in fractured systems [*Neretnieks and Rasmuson*, 1984; *Moench*, 1995; references cited in *Haggerty et al.*, this issue], construction of a continuous multirate mass-transfer model from TWCF tracer-test data has not previously been reported.

The goal of this paper is to elucidate the processes responsible for mass transfer in the Culebra dolomite. Toward this goal, we are interested in developing a model of mass transfer between fracture and matrix porosity, or more generally between advective porosity and diffusive porosity, and testing that model on data acquired in a number of TWCF tracer tests. In this paper we will: (1) extend the methodology of estimating distributions of multirate mass transfer rates from the SWIW to the TWCF tests; (2) model the observed TWCF breakthrough curves with a multirate diffusion model; (3) examine the uniqueness of the estimated model and compare the results to those obtained with conventional single-rate models; and (4) discuss the extension, or scale-up, of the multirate model to scales larger than that of the multiwell tracer test (i.e., the scale of repository performance assessment).

Multirate Transport Modeling in Two Well Systems

The multirate diffusion transport model described in *Haggerty et al.* [this issue] is extended here to work with TWCF tests. The multirate model [*Haggerty and Gorelick*, 1995] enables mass transfer to be modeled with a continuous distribution of diffusion rate coefficients. A distribution of diffusion rate coefficients may arise from variability in the following: matrix block sizes, cross-sectional area of the pore space normal to the direction of diffusion and tortuosity. The multirate mass transfer model presented here is similar to that described by *Cunningham et al.* [1997] and *Haggerty and Gorelick* [1998] . Diffusion is assumed to occur along one-dimensional pathways within the matrix blocks and it is assumed that mass-transfer properties are homogeneous along each pathway and that the pathways are independent of all

other pathways. The pathways and matrix blocks can be any shape as long as the diffusion rate coefficients form a continuous distribution. In this work, we employ a log-normal distribution of diffusion rate coefficients for reasons discussed in *Haggerty and Gorelick* [1998] and for direct comparison to SWIW tracer test results [*Haggerty et al.*, this issue].

In the TWCF tracer tests considered here, a steady-state convergent-flow field is obtained by pumping from an extraction well. Tracer injection occurs as a pulse/slug into the convergent-flow field at an injection well located at some radial distance, R_o, away from the pumping well. A chaser of clean (no tracer) fluid is injected immediately following the tracer injection to ensure that no tracer is left in the injection borehole. The aquifer is assumed to be fully confined with constant thickness in all directions and to have spatially isotropic and homogeneous flow and transport properties. Mechanical mixing due to small-scale variations in the flow field is approximated with a dispersivity term. The regional gradient is considered to be negligible. Given these conditions, the process of solute transport into or out of a well is described by:

$$\frac{\partial c_a}{\partial t} + \int_0^\infty b(\alpha_d)\frac{\partial \hat{c}_d(\alpha_d)}{\partial t} d\alpha_d = \frac{1}{r}\frac{\partial}{\partial r}\left(\frac{r\alpha_l |v|}{R_a}\frac{\partial c_a}{\partial r}\right) - \frac{v}{R_a}\frac{\partial c_a}{\partial r} \tag{1}$$

where the distribution of diffusion rates is represented as a probability density function of diffusion rate coefficients, $b(\alpha_d)$, defined by a lognormal distribution:

$$b(\alpha_d) = \frac{\beta_{tot}}{\sqrt{2\pi}\sigma_d \alpha_d}\exp\left\{\frac{[\ln(\alpha_d) - \mu_d]^2}{2\sigma_d^2}\right\} \tag{2}$$

where

$$\alpha_d = \frac{D_a}{l^2} \tag{2b}$$

and

$$\beta_{tot} = \frac{\phi_d R_d}{\phi_a R_a} \tag{2c}$$

where c_a [M/L^3] is the solute concentration in the advective porosity (e.g., fractures); $c_d(\alpha_d)$ [M/L^3] is the average solute concentration in the portion of the matrix associated with a particular diffusion rate coefficient; α_d [$1/T$] is the diffusion rate coefficient defined by (2b), which is continuously distributed; β_{tot} [-] is the total capacity coefficient of the formation, which is the

ratio of the solute mass in the diffusive porosity to solute mass in the advective porosity at equlibrium; α_l [L] is the longitudinal dispersivity along the flow path; v [L/T] is the pore-water velocity; R_a [-] is the retardation factor in the advective porosity; r[L] is the radial coordinate (positive away from the well); t [T] is time elapsed since the beginning of injection of the first tracer; σ_d is the standard deviation of the log-transformed diffusion rate coefficients; μ_d is the natural log of the geometric mean of the diffusion rate coefficients; D_a [L^2/T] is the apparent matrix diffusion coefficient, defined for this work as the product of the aqueous diffusion coefficient and the diffusive tortuosity; l [L] is the length of the diffusion pathway within the matrix; ϕ_d [-] is the diffusive porosity of the formation; R_d is the retardation factor due to sorption within the diffusive porosity; and ϕ_a is the advective porosity.

A distribution of mass-transfer rates arising from variation in block sizes is geologically more plausible than the single matrix block size ("sugar cube") conceptualization employed in standard double porosity models. Equation 2 not only defines this distribution of diffusion rate coefficients, lognormal in this work, but provides a critical link between the diffusion rate coefficients and the solute storage capacity of the diffusive porosity associated with each rate coefficient. Equation 2 ties each diffusion rate coefficient, α_d, to a specific volume of storage. This volume is specified as a fraction of the total storage capacity of the medium, β_{tot}, and is expressed as a function of the diffusion rate coefficient $\beta(\alpha_d)$. For non-sorbing tracers, $\beta_{tot} \equiv \phi_d / \phi_a$. Also, variability in α_d is due to variability in both l and τ (2b) and the joint variability cannot be further refined

The time derivative of the spatially averaged solute concentration in the matrix is given by

$$\frac{\partial \hat{c}_d(\alpha_d)}{\partial t} = \frac{1}{l}\int_0^l \frac{\partial c_d(\alpha_d)}{\partial t} dz, \; 0 < \alpha_d < \infty \qquad (3a)$$

where c_d [M/L^3] is the concentration at a point within a portion of the diffusive porosity (matrix) associated with a certain diffusion rate coefficient; and z [L] is the coordinate along the one-dimensional diffusion pathway. This concentration at a point within the diffusive porosity is given by a solution to the diffusion equation:

$$\frac{\partial c_d(\alpha_d)}{\partial t} = D_a \frac{\partial^2 c_d(\alpha_d)}{\partial z^2}, \quad 0 < \alpha_d < \infty \tag{3b}$$

The boundary condition for diffusive mass transfer is that the concentration at the edge of the diffusive porosity (matrix) is equal to the concentration in the advective porosity (fracture):

$$c_d(\alpha_d) = c_a, \quad 0 < \alpha_d < \infty \tag{3c}$$

To solve these equations, we use the approach developed by *Haggerty and Gorelick* [1995, 1998] where a series of first-order equations are used in place of (3a) and (3b) [see *Haggerty et al.*, this issue, appendix A]. These equations are solved in the Laplace-domain and then numerically inverted back to the time domain. The resulting solution for c_d from the first-order equations is mathematically identical to that which would be obtained if solving the above equations directly.

Boundary conditions and fluid velocities must also be specified at the injection well. Pore-water velocity during the injection of the tracer and chaser fluid at a radius, r, away from the injection well is given by

$$v = \frac{Q_{inj}}{2\pi r \phi_a b} \tag{4}$$

where Q_{inj} [L^3/T] is the rate of injection for the tracer or chaser and b [L] is the aquifer thickness. The boundary conditions for use with (1) under radially divergent flow are:

$$c_a - \alpha_L \frac{\partial c_a}{\partial r} = c_{inj} \quad \text{at } r = r_w \tag{5a}$$

$$\frac{\partial c_a}{\partial r} = 0 \quad r \rightarrow \infty \tag{5b}$$

The combined shape of the injected tracer and chaser within the aquifer is assumed to be unaffected by the convergent-flow field during the time of injection (i.e., solute forms a perfect

ring around the injection well). In general, this assumption remains valid if (1) the ratio of the volume of fluid injected to the volume of fluid contained within a single pore volume within the area defined by the two wells is small and (2) the ratio of fluid velocity caused by injection to fluid velocity due to pumping is large at the location of the injection well. These two constraints can be expressed, respectively, as [after *Guvanasen and Guvanasen*, 1987]:

$$\frac{Q_{inj1} * T_{inj1} + Q_{inj2} * T_{inj2}}{b\phi_a \pi R_o^2} << 1 \qquad (6a)$$

$$\frac{Q_{inj} R_o}{Q_{out} R_{iw}} >> 1 \qquad (6b)$$

where Q_{inj1} and Q_{inj2} refer to the injection rates of the tracer and chaser respectively, T_{inj1} and T_{inj2} refer to the elapsed time of injection for the tracer and chaser respectively, and R_{iw} is the radius of the injection well. The injection rate denoted as Q_{inj} in (6b) is taken as the larger of the two injection rates (tracer or chaser) and Q_{out} refers to the discharge rate of the pumping well. We will use the equations described above to test the conceptual model of multirate diffusion against observed tracer test data, but first it is necessary to devise a means of modeling the movement of tracer along the transport pathway from the injection well to the pumping well.

A three-step process is used to determine the breakthrough curve at the pumping well after the initial injection of tracer and chaser. The first step is to transform the post-injection concentration distribution from polar coordinates centered on the injection well (r_{in}, θ_{in}) to polar coordinates centered on the pumping well (r_{out},θ_{out}). The second step is to reduce the dimensionality of the problem through azimuthal averaging. The final step in simulating the breakthrough curve is to model the transport through the aquifer to the pumping well under a radially convergent-flow field with the multirate diffusion model described in (1) through (5). Completion of these three steps provides a semi-analytical solution for the BTC at the pumping well.

Step one involves transformation of the polar coordinates from the injection well to the pumping well. Figure 1 shows the relationship between the polar coordinate system with respect to the two wells along with an intermediate cartesian coordinate system. The transformations from the injection well coordinate system to the pumping well coordinate system are:

$$r_{out} = \sqrt{R_o + 2R_o r_{in} \cos\theta_{in} + r_{in}^2} \tag{7a}$$

$$\theta_{out} = \tan^{-1}\left(\frac{r_{in}\sin\theta_{in}}{R_o + r_{in}\cos\theta_{in}}\right) \tag{7b}$$

Second, we reduce the dimensionality from two to one. Solute transport toward the pumping well as shown in Figure 1 would require solution of a system of integro-differential equations in r_{out}, θ_{out} and t. Azimuthal averaging can eliminate θ_{out} from this transport problem [*Zlotnik and Logan*, 1996]. Azimuthal averaging takes all concentrations at a distance r from the pumping well and averages them. In a formation with uniform thickness, advective porosity and hydraulic conductivity, all mass at a given radial distance from the pumping well will experience the same velocity and similar dispersion as it moves toward the well. Therefore, all concentrations at a distance r from the pumping well can be averaged and transport simulated in one dimension rather than two. The azimuthally averaged concentration at the end of the injection period, time = t_o, (beginning of convergent-flow only period) is given by [*Zlotnik and Logan*, 1996]:

$$C(r_{out}, t_o) = \frac{1}{2\pi}\int_{-\pi}^{\pi} c(r_{out}, \theta_{out}, t_o)\, d\theta_{out} \tag{8}$$

where r_{out} [L] is the distance from the pumping well and θ_{out} is the angle between the mass at r_{out} and the axis intersecting the pumping and injection wells. It is not necessary to integrate (8) over the entire interval $[-\pi,+\pi]$, but only over the interval where there is non-zero concentration. Azimuthally averaged concentrations are also obtained for the matrix. After the azimuthal averaging of concentrations, transport to the pumping well is modeled using (1) through (5).

The ability of the multirate model to estimate the diffusion rate coefficient distribution is limited by the ratio of diffusive to advective mass-transfer rates within the tracer test system. The ratio of diffusive to advective mass transfer can be parameterized with the Damkohler number, *DaI*. For a one-dimensional flow system with first-order mass transfer, the type 1 Damkohler number is [*Haggerty and Gorelick*, 1995]:

$$DaI = \alpha_f (\beta(\alpha_f) + 1) \frac{R_a L}{v} \tag{9a}$$

where a_f [1/T] is the first-order mass-transfer coefficient, $\beta(\alpha_f)$[-] is the capacity coefficient, L [L] is the length of the flowpath, R_a [-] is the retardation coefficient in the advective porosity and v [L/T] is the pore velocity of the water. In a system with diffusion, (9a) must be modified. Several papers, starting with *Glueckauf* [1955], have suggested that diffusive mass transfer can be approximated by first-order mass transfer. For diffusion into layers, this linear driving force approximation is made by setting α_f equal to $3\alpha_d$ [*Goltz and Roberts*, 1987]. Therefore, we modify the Damkohler expression accordingly:

$$DaI = 3\alpha_d (\beta(\alpha_d) + 1) \frac{R_a L}{v} \tag{9b}$$

Damkohler numbers near 1 indicate that the rate of diffusion is similar to the rate of advection. At a Damkohler number of 100, diffusion can be considered instantaneous relative to advection and the local equilibrium assumption (LEA) applies [*Bahr and Rubin*, 1987]. Conversely, at a Damkohler number of 0.01, diffusion is negligible relative to advection and a single porosity (ϕ_a) conceptualization of the transport problem will apply.

The Damkohler number can be examined across the distribution of mass-transfer rates in a radial flow system by considering the average velocity along a flowpath from an arbitrary starting radius, R_o, to the extraction well radius, r_w. For a radial flow system at steady state, the average advective velocity along a flowpath is the distance between the injection and pumping wells divided by the time it takes to pump one pore volume from the cylinder defined by R_o and the aquifer thickness, b. This time is expressed as the pore volume of the cylinder divided by the

discharge rate at the pumping well, Q. After algebraic reduction, this temporally averaged velocity, $\bar{v}$, is:

$$\bar{v} = \frac{Q(R_o - r_w)}{\pi(R_o^2 - r_w^2)b\phi_a} \tag{10}$$

This average flowpath velocity is used in (9b) to determine the Damkohler number across the distribution of mass-transfer rates. The Damkohler number is used below to determine the limits of diffusion coefficients that can be resolved by the TWCF tests and to examine the effect of a multirate model at scales larger than those of the tracer tests.

Results of TWCF Tracer Test Simulations

Two pumping-injection well pairs are analyzed and each well pair is analyzed at two different pumping rates. The H-11 and H-19 pathways (H-11 [b3 to b1] and H-19 [b7 to b0]) were selected because high quality data were available for both the high and low pumping rates. Each pair of injection/withdrawal wells provides a full set of benzoic acid tracer data for each of two different pumping rates. The different benzoic acid tracer tests will be referred to by the hydropad name and the relative pumping rate for the remainder of this paper (e.g., "H-19 high"). The parameters that are set as fixed values in the models are given in Table 1. All fluid and tracer injections and withdrawals were done across the full aquifer thickness. Further details regarding the physical setup and data collection of the tracer tests can be found in *Meigs and Beauheim* [this issue].

Experimental Data

The H-11 low pumping rate test (H-11 low) was run at a constant pumping rate for approximately 25 days after injection of the tracer. During this time period, 107 samples were collected and analyzed for concentration. For the higher pumping rate test (H-11 high), a total of 75 samples were collected to define the breakthrough curve. These samples and the upper and lower limits of the 95 percent confidence interval based on analytical error are shown in Figure 2. All BTC concentration data shown in this paper are normalized by the injection concentration (C/C_o).

For the H-19 low tracer test, 67 samples were used in the parameter estimation. For the H-19 high test, 28.8 days of observed data were used in the modeling results presented here (total of 77 data points). The H-19 BTC's and the 95 percent confidence interval based on analytical error are shown in Figure 3.

Parameter Estimation

Parameter estimation applied to the multirate diffusion model discussed above is used to provide an optimal fit of the model to the observed data. The parameter estimation minimizes the root mean square error (RMSE) between the log of the observed data and the log of the predicted concentration. Four parameters are estimated: the mean *ln* diffusion rate coefficient, μ_d; the standard deviation of the *ln* diffusion rate coefficient distribution, σ_d; the advective porosity, ϕ_a; and the longitudinal dispersivity, α_l. The parametric expression of diffusion rate coefficients used here is a log-normal distribution fully characterized by the mean and standard deviation. In addition to the four parameters, normalized sensitivity of the results to each estimated parameter is calculated.

The inverse parameter estimation model creates a matrix containing the sensitivity of concentration change with respect to each parameter for each observation time. The entries of this Jacobian may be normalized to allow comparison of parameter sensitivities through time and between different parameters [*Harvey et al.*, 1996]:

$$J_{ij} = \frac{p_j}{\sigma}\frac{\partial C_i}{\partial p_j} \tag{11}$$

where J_{ij} is the normalized sensitivity of the modeled concentration at the i^{th} time to the j^{th} parameter, C_i is the i^{th} component of the vector of normalized concentrations through time, p_j is j^{th} component of the vector of estimated parameters, and σ is the estimated standard deviation for the concentration observations. Here we assume that errors are uncorrelated and due to measurement error rather than model error and thus we use RMSE in (11) as a measure of σ. The Jacobian is a useful instrument for investigating the sensitivity through time of the model to the estimated parameters [e.g., *Wagner and Harvey*, 1997], and gives insight into the correlation between estimated parameters.

The normalized sensitivities of the H-11 low test are shown as an example of normalized sensitivities in the TWCF tests (Figure 4). Examination of the normalized sensitivities shows that the model of the TWCF tests is relatively insensitive to the values of σ and α_l after the time of peak concentration (approximately 0.6 days for the H-11 low test). Beyond this time, the model is only sensitive to the mean diffusion rate coefficient, μ_d and ϕ_a (Figure 4).

The estimated parameter values and the RMSE statistic obtained with the multirate model are given for the H-11 and H-19 tests in Table 2. The 95 percent confidence intervals in Table 2 are approximated as +/- 2 standard deviations about the estimated value. For σ_d, ϕ_a and α_l, the confidence interval is taken about the natural log of the estimated value as these three parameters are estimated in natural-log space within the parameter estimation algorithm. Examination of Table 2 shows that the RMSE values are all relatively small, indicating that the models provide a good fit to the observed data. Figures 5 and 6 compare the model results to the observed data for the H-11 and H-19 TWCF tests respectively. From Figures 5 and 6, it can be seen that the models approximate the data best at times after the peak concentration when diffusion of solute back out of the diffusive porosity into the advective porosity is the dominant mass-transfer process.

Discussion of Results

Results shown in Figures 5 and 6 are based on estimated log-normal distributions of diffusion coefficients. At both hydropads, the tracer test conducted at the lower pumping rate produces a lower estimate of the mean diffusion rate (μ_d). The cumulative diffusive porosity volume as a function of diffusion rate coefficient as determined from the inverse parameter estimation using the multirate model is shown in Figure 7 for both rounds of tests at both hydropads. Examination of Figure 7 shows that for the two hydropads, the estimated distribution of diffusion rate coefficients is similar from one pumping rate to the other. However, the estimated distributions for the H-11and H-19 hydropads differ significantly. A similar result was observed in the evaluation of the SWIW tests [*Haggerty et al.*, this issue].

The portion of the log-normal distributions that can actually be resolved during the tests is determined by applying the Damkohler number limits of 0.01 and 100. At the H-11 hydropad roughly 99 percent of the diffusion rate distribution lies within the 0.01 and 100 Damkohler number limits with just the slowest one percent of the rates lying below the 0.01 cutoff. At the

H-19 hydropad, approximately 59 percent of the distribution lies within the limits as shown by the bold portion of the line in Figure 7. Consequently, at the H-19 hydropad approximately 29 percent of the estimated diffusion rates are so slow as to be negligible and approximately 12 percent of the rates are fast enough to appear instantaneous. The large confidence intervals about the estimates of σ_d, shown in Table 2 for H-19, are due to the large proportion of the estimated mass-transfer coefficient distribution that lies outside the limits imposed by the Damkohler number. The distribution is effectively unestimable outside these limits and only has shape in those regions (Figure 7) because of the *a priori* assumption of a log-normal distribution.

Relatively larger confidence intervals are estimated for α_l in the H-11 low test. We believe that this imprecise estimate is caused by the rapid transport of the tracer to the pumping well (peak concentration is achieved in less than 9 hours after injection) and the insensitivity of the models to α_l beyond the time of peak concentration. Longer times to peak concentration in the H-11 high and H-19 tests allow for more precise determination of α_l.

The consistency of the estimated, log-normal distributions of mass-transfer rates can be checked by determining the estimated matrix block size distribution. All variability in the mass transfer rates is assigned to variations in matrix block size by assuming a constant tortuosity and then comparing estimated matrix block lengths to field observations. For one-dimensional diffusion paths into the matrix, the distance from the fracture/matrix to the center of the matrix block, l, (matrix block 1/2 length) can be calculated as:

$$l = \sqrt{\frac{D_o \tau}{\alpha_f}} \tag{12}$$

where D_o [L^2/T] is the aqueous diffusion coefficient, τ is the tortuosity[-], and a_f [$1/T$] is the first order mass-transfer coefficient. Using the values of D_o and τ in Table 1, the resulting distributions show that these tests were able to image, within the Damkohler limits, a range of half-block sizes from < 0.001 to 0.09 meters at the H-11 hydropad and from 0.0004 to 0.06 meters at the H-19 hydropad. These estimates of block size are consistent with the lower end of the range of block sizes observed in core and outcrop samples [*Holt*, 1997].

The observed BTC data show similar peak concentrations for both pumping rates. This behavior is generally characteristic of a single-porosity aquifer, provided the difference in pumping rates is large enough to change the peak concentration significantly. In a mulitrate system characterized by a log-normal distribution of diffusion coefficients, the change in peak height between different pumping rates decreases as σ_d increases. Using the parameters estimated at H-19 ($\sigma_d > 5.0$), numerical simulations show a constant peak height across pumping rates that change by up to one order of magnitude. Similar simulations using the parameters estimated at H-11 (σ_d near 1.0) show a change in peak concentration across the same range of pumping rates. We are currently evaluating different parametric and non-parametric, including bimodal, distributions of diffusion coefficients to understand better the similarity in peak concentrations across different pumping rates.

Alternative Conceptual Models

The multirate mass-transfer model provides reasonable matches to the data observed in the TWCF tests. Additionally, the multirate model is consistent with observed matrix block sizes. However, we considered that the BTC's could result from either a single-porosity model with a heterogeneous transmissivity field or from a single-rate double-porosity model. Both of these alternative conceptual models are tested as explanations for the observed TWCF test results.

Single-Porosity Heterogeneous-Transmissivity Model

A series of numerical experiments was conducted to examine the character of tracer BTC's in heterogeneous, single-porosity domains. The heterogeneous fields were created with both maximum entropy and indicator geostatistical simulation techniques [see *Journel and Deutsch,* 1993] using a variety of correlation lengths. The spatial correlation of the fields was isotropic as determined by analysis of hydraulic tests at H-19 [*Beauheim and Ruskauff*, 1998] and a range of advective porosities from 0.05 to 5×10^{-4} was used. Flow and transport were simulated through each heterogeneous field using a particle tracking transport algorithm [*Tsang,* 1995] and the time to 90 percent mass recovery of the resulting BTC's was compared against data observed at H-19. These simulations are documented in *Meigs et al.* [in review]. The time to 90 percent mass recovery in all single-porosity simulations was significantly faster (factor of 2 or more) than in

the observed data. These results suggest that a mass-transfer process is necessary to create the BTC tailing observed in the data.

Single-Rate, Double-Porosity Model

Previous to this work, only single-valued diffusion rates have been applied to the analysis of two-well, double-porosity tracer tests. To compare the results of the multirate model to the conventional, single-rate (double porosity) approach, single-rate model runs were completed using parameter estimation for the low pumping rate tracer test at each hydropad. This estimation procedure is the same as that used for the multirate model; however, σ_d is set to 0.0. In order to maintain consistency, these single-rate runs were constrained to have the same total porosity ($\phi_a + \phi_d$) as derived from the multirate modeling. Results of the single-rate matches to the observed data are given in Table 3 and Figures 8 and 9.

In general, the single rate of mass transfer is smaller (larger negative number) than the mean of the multirate distribution for both of the TWCF tests modeled. The estimated mass-transfer rate using the conventional double-porosity model results in matrix half-block sizes of 0.16 and 0.32 meters at the H-11 and H-19 hydropads, respectively. For the H-19 test, the advective porosity estimated with a single-rate model is over an order of magnitude larger than that estimated with the multirate model (Table 3). As measured by the RMSE, the multirate model provides a better fit to the data than does the single-rate model for both the H-11 and H-19 tests. The RMSE is approximately a factor of 2 lower for the multirate model of the H-11 data; however, the improvement in the fit to the data is only marginal for the H-19 test.

The Damkohler numbers calculated with a single-rate model change in inverse correspondence to the change in average velocity between pumping rates. The Damkohler numbers estimated based on the single-rate model at the lower pumping rates are 4.4×10^{-2} and 4.1×10^{-3} for the H-11 and H-19 tests, respectively. For the length of time that these tracer tests were run, these low Damkohler numbers indicate that the single-rate model considers diffusion into the matrix to be extremely small to negligible. Conversely, the multirate model estimated relatively rapid to instantaneous rates for a significant fraction of the total porosity. In the H-11 models, there is no significant increase in the fracture porosity from the multirate results to the single-rate results. Results of the H-19 models show that the advective porosity estimated in the single-rate case is over an order of magnitude higher than the value estimated in the multirate

model. In order to account for the instantaneous diffusion rates resolved by the multirate model, the single-rate model predicts a higher advective porosity relative to the multirate model. Over the length of the tracer test, a fraction of the matrix will become saturated with solute due to "fast" diffusion rates. In the single-rate model, this process is accounted for by assigning that fraction to the advective porosity.

Uniqueness and Testing of the Estimated Models

A test of the robustness or validity of the estimated multirate transport model is to use the transport parameters estimated at one pumping rate to model the observed BTC at the other pumping rate. If the conceptual model of a continuous distribution of diffusion rate coefficients holds, the change in pumping rate will shift the portion of the diffusion rate coefficient distribution that the test is able to see (that region between seemingly infinite block size and LEA behavior). In the case of a continuous diffusion rate coefficient distribution, the corresponding distribution of Damkohler numbers can remain approximately constant with a change in pumping rate by activating a different portion of the diffusion rate coefficient distribution. However, if the single mass-transfer rate model applies, there are no other rates to shift to and the single Damkohler number will change with changing pumping rates giving different transport results. If this change in *DaI* is significant, then matching the BTC using transport parameters from tests at a different pumping rate will not be possible.

The observed data at the higher pumping rates are modeled using both the continuous distribution of diffusion rates estimated at the lower pumping rate and also using the single diffusion rate estimated at the lower pumping rate with a single-rate model. The results of these runs are shown with the observed data in Figures 10 and 11. The RMSE for the fits shown in Figure 10 (H-11 tracer test) are 0.26 and 0.30 for the single-rate and multirate models respectively. The RMSE values for the models shown in Figure 11 (H-19 tracer test) are 0.33 and 0.24 for the single-rate and multirate models respectively. In both cases, the single-rate model estimated at the lower pumping rate is capable of matching the data observed at the higher pumping rate as well as the multirate model. These results are not surprising given that the higher pumping rates lower the Damkohler number by roughly a factor of two. The calculated Damkohler numbers are already indicating negligible diffusion at the low pumping rate and the potential for diffusion is even less at a higher advection rate. If a larger difference in pumping

rates had been used in the field test, it might have been possible to differentiate between the two models.

Comparison of SWIW and TWCF test results

Results of modeling the TWCF tests are compared to those of the SWIW tests with the goal of understanding the differences in the estimated parameters in terms of the differences in the two tracer test designs. We do not expect that the results of the different tests will be completely comparable because of the different test geometries and, to a large extent, non-overlapping volumes of aquifer being tested. Additionally, the TWCF tests are more sensitive to ϕ_a and α_l than are the SWIW tests. For example, the SWIW test is completely insensitive to the value of advective porosity (see Table 2, *Haggerty et al.*, this issue), but ϕ_a is estimated with relatively tight confidence intervals by models of the TWCF tests (Table 2).

Comparison of Table 2 in *Haggerty et al.* [this issue] with Table 2 in this paper shows that the estimates of μ_d from the SWIW and TWCF tests are similar at H-11 and quite different at H-19. At H-19, the estimates of the mean diffusion rate coefficient by the SWIW model are approximately two orders of magnitude higher than those estimated by the TWCF model. One explanation for the large differences between the SWIW and TWCF tests at H-19 is the time available for diffusion. The normalized sensitivities (see Figure 4) indicate that for times beyond the peak concentration, the main process affecting the BTC is diffusion back out of the diffusive porosity into the advective porosity. The elapsed time from beginning of tracer collection to peak concentration in the BTC is used as a representative time for diffusion to occur. At H-11, this representative time is approximately 75,000 seconds for the SWIW test and roughly 45,000 seconds for the TWCF test. However, at H-19, this representative time for diffusion is almost an order of magnitude longer in the TWCF tests (3.5×10^5 to 6.0×10^5 seconds) than in the SWIW tests (approximately 75,000 seconds). These similar times for diffusive mass transfer at H-11 across both tests result in models that predict similar values for μ_d (see Table 2). The longer time for diffusion in the H-19 TWCF tests relative to the SWIW tests allows the tracer to sample slower diffusion rates, and these slower rates significantly decrease the estimated mean of the diffusion rate coefficient distribution relative to the SWIW test.

Mass-Transfer Processes at Larger Scales

The final goal of determining mass-transfer rates within the Culebra dolomite, and many aquifers examined by tracer testing, is use of the estimated parameters in a solute transport model for predictions of transport processes at larger spatial and temporal scales. These calculations may be performed on spatial scales of kilometers and temporal scales of hundreds to thousands of years. This raises the question of the effect a multirate mass-transfer process might have on the shape of a solute plume at various distances downgradient of the solute source relative to that predicted by a conventional single-rate double-porosity model.

At larger time and length scales, two differences between the single-rate and multirate models estimated in this work must be considered: 1) single-rate models may indicate a larger advective porosity than do the multirate models and 2) slow rates in the tail of the multirate diffusion coefficient distribution may cause at least a fraction of the diffusive porosity to remain unsaturated with solute even at very large times. The significance of these differences is analyzed by calculating the Damkohler number (equation 9b) at transport distances of 300 and 3000 meters using the estimated distributions of diffusion rate coefficients.

A specific discharge of 1×10^{-8} m/s is used with the multirate distributions estimated for the H-11 and H-19 Low tracer tests to calculate a cumulative distribution of Damkohler numbers. For the estimated H-11 diffusion coefficient distribution, the Damkohler numbers are all greater than 0.01 at both 300 and 3000 meter transport distances. At a transport distance of 300 meters, approximately 77 percent of the total matrix capacity is saturated ($DaI > 100$) and at 3000 meters, more than 99 percent of the capacity is saturated. For this distribution, there is no fraction of the storage capacity with seemingly infinite matrix block sizes ($DaI < 0.01$); while not saturated with solute, there would be a non-zero solute concentration at the center of all matrix blocks. Saturation of such a large fraction of the matrix coupled with no extremely slow diffusion rates creates transport results that are indistinguishable from the single-rate model at both 300 and 3000 meters. Given the estimated H-11 distribution of diffusion coefficients, we could conceptualize transport through the Culebra as occurring in a single-porosity system with an effective porosity of 77 or > 99 percent of the total porosity ($\phi_a + \phi_d$) for the 300 and 3000 meter transport distances, respectively.

The estimated diffusion coefficient distribution from the H-19 tracer tests has a much broader σ_d value and, thus, a fraction (less than 2 percent) of the diffusion rates are slow enough to appear as seemingly infinite matrix block sizes at both the 300 and 3000 meter transport distances. These extremely slow rates cannot occur in the single-rate model, and transport results are different for the single-rate and H-19 multirate parameters at both 300 and 3000 meter transport distances. It is not possible to accurately model transport in the Culebra, as parameterized using the H-19 tracer test results, with a single porosity conceptualization. The single-porosity model, exhibiting complete saturation of the matrix, may be a non-conservative (i.e., low) estimate of the cumulative release of solute across a regulatory boundary.

Conclusions

The multirate diffusion model developed previously [*Haggerty and Gorelick*, 1995] is extended to the case of a convergent-flow system with an injection at some distance from the pumping well. This model has been applied to a portion of the results from the H-11 and H-19 tracer tests conducted in the Culebra dolomite at the WIPP site. Parameters estimated from modeling the observed data suggest that the diffusion process is different from one hydropad to the other. For the pathway evaluated at the H-11 hydropad, the estimated values of α_L are greater than 15 percent of the length of the transport pathway, while for the pathway evaluated at the H-19 hydropad these values are less than 10 percent of the pathway length. At H-11, the confidence intervals on the estimated σ_d values are relatively tight while the confidence intervals on σ_d at H-19 are quite large and indicate that σ_d is unestimable at H-19. The confidence intervals on ϕ_a are narrow at both hydropads.

Results of this work indicate that evidence of multirate diffusion is best determined by the SWIW tracer test. In a SWIW test, the effects of flow field heterogeneity are mitigated and the signature of multirate diffusion is easily detectable. In the case of the TWCF tracer tests, both a single-rate and multirate model are capable of describing the observed data. The added effects of flow field heterogeneity and correlation of the mean diffusion rate with the advective porosity in the TWCF tests make the interpretation of the diffusion process more ambiguous.

Parameters derived with data from a SWIW test are not necessarily transferable to a TWCF test. The fast end of the diffusion rate distribution is better estimated with a SWIW test because

of the insensitivity of that test to advective porosity. For a TWCF test, it can be difficult to differentiate between very fast diffusion rates and advective porosity. At H-19, the insensitivity of the SWIW test to advective porosity made it impossible to simulate the test data with a single-rate model. However, the H-19 TWCF test can be simulated using an increased advective porosity to account for the instantaneous diffusion and fitting the data with a single-rate model.

At larger transport scales, the width of the estimated multirate diffusion coefficient distribution will dictate whether or not a single-porosity model can accurately model the transport behavior for a given transport distance. Based on the parameters estimated in this work, a single-rate conceptualization may predict a smaller cumulative release across a regulatory boundary, relative to a multirate model, due to the entire matrix becoming saturated with solute. If very slow diffusion rates are present in the multirate model, a fraction of the matrix may remain unsaturated and the cumulative releases across the regulatory boundary will be larger. An unsaturated matrix can also be maintained at larger scales with a single-rate model if a slower diffusion rate is chosen. At large transport scales, the fast diffusion rates will have reached equilibrium, saturating the associated fraction of the total capacity. Whether this fraction of the total capacity is accounted for explicitly in the transport model, or just assigned as advective porosity, does not make a difference for the cases examined here.

Acknowledgements

Sandia is a multiprogram laboratory operated by Sandia Corporation, a Lockheed Martin Company, for the United States Department of Energy under Contract DE-AC04-94AL85000. This paper was improved through the reviews of V. Tidwell, T. Corbet, P. Davies and R. Beauheim, and discussions with S. Altman, S. Fleming, and R. Holt. Some of the calculations herein were done by M. Kelley, T. Jones and J. Ogintz.

References

Altman, S.J., L.C. Meigs, and T.L. Jones, Tracer tests in a fractured dolomite, 2. Evaluation of the importance of matrix diffusion, *Water Resour. Res.*, this issue.

Bahr, J.M. and J. Rubin, Direct comparison of kinetic and local equilibrium formulations for solute transport affected by surface reactions, *Water Resour. Res., 23* (3), 438-452, 1987.

Beauheim, R.L. and G.J. Ruskauff, Analysis of hydraulic tests of the Culebra and Magenta dolomites and Dewey Lake Redbeds conducted at the Waste Isolation Pilot Plant site, *SAND98-0049*, Sandia National Laboratories, Albuquerque, New Mexico, 1998.

Cunningham, J.A., C.J. Werth, M. Reinhard, and P.V. Roberts, Effects of grain-scale mass transfer on the transport of volatile organics through sediments: 1. Model Development, *Water Resour. Res., 33* (12), 2713-2726, 1997.

D'Alessandro, D., F. Mousty, G. Bidoglio, J. Guimerà, I. Benet, X. Sánchez-Vila, M. García Gutiérrez, and A. Yllera De Llano, Field tracer experiment in a low permeability fractured medium: results from El Berrocal site, *J. Contam. Hydrol., 26*, 189-201, 1997.

Glueckauf, E., Theory of Chromotography, Part 10, Formulae for diffusion into spheres and their application to chromatography, *Trans. of the Faraday Soc., 51*, 1540-1551, 1955.

Goltz, M.N. and P.V. Roberts, Using the method of moments to analyze three-dimensional diffusion-limited solute transport from temporal and spatial perspectives, *Water Resour. Res., 23* (8), 1575-1585, 1987.

García Gutiérrez, M.G., J. Guimerà, A. Yllera De Llano, A. Hernàndez Benitez, J. Humm, and M. Saltink, Tracer test at El Berrocal Site, *J. Contam. Hydrol., 26*(),179-188, 1997.

Guvanasen, V. and V.M. Guvanasen, An approximate semianalytical solution for tracer injection tests in a confined aquifer with a radially converging flow field and finite volume of tracer and chase fluid, *Water Resour. Res., 23* (8), 1607-1619, 1987.

Hadermann, J., and W. Heer, The Grimsel (Switzerland) migration experiment: Integrating field experiments, laboratory investigations and modeling, *J. Contam. Hydrol., 21*, 87-100, 1996.

Haggerty, R. and S.M. Gorelick, Mulitple rate mass-transfer for modeling diffusion and surface reactions in media with pore-scale heterogeneity, *Water Resour. Res., 31* (10), 2383-2400, 1995.

Haggerty, R. and S.M. Gorelick, Modeling mass transfer processes in soil columns with pore-scale heterogeneity, *Soil Sci. Soc. Am. J.*, *62* (1), 62-74, 1998.

Haggerty, R., S.W. Fleming, L.C. Meigs, and S.A. McKenna, Tracer tests in a fractured dolomite, 3. Analysis of mass transfer in single-well injection-withdrawal tests, *Water Resour. Res.*, this issue.

Harvey, J.W., B.J. Wagner, and K.E. Bencala, Evaluating the reliability of the stream tracer approach to characterize stream-subsurface water exchange, *Water Resour. Res.*, *32* (8), 2441-2451, 1996.

Holt, R.M., Conceptual model for transport processes in the Culebra Dolomite Member, Rustler Formation, *SAND97-0194*, Sandia National Laboratories, Albuquerque, New Mexico, 1997.

Journel, A.G. and C.V. Deutsch, Entropy and spatial disorder, *Math. Geol.*, *25* (3), 329-355, 1993.

Meigs, L.C. and R.L. Beauheim, Tracer tests in a fractured dolomite, 1. Experimental design and observed tracer recoveries, *Water Resour. Res.*, this issue.

Meigs, L.C., S.A. McKenna, S.J. Altman, R.L. Beauheim, J.T. McCord, R. Haggerty, S.W. Fleming, T.L. Jones, J. Ogintz, and I. Farnham, Interpretations of tracer tests performed in the Culebra dolomite at the Waste Isolation Pilot Plant site, SAND97-3109, Sandia Natl. Lab., Albuquerque, NM, in review, expected publication 1999.

Moench, A.F., Convergent radial dispersion: A Laplace transform solution for aquifer tracer testing, *Water Resour. Res.*, *25* (3), 439-447, 1989.

Moench, A.F., Convergent radial dispersion in a double-porosity aquifer with fracture skin: Analytical solution and application to a field experiment in fractured chalk, *Water Resour. Res.*, *31* (8), 1823-1835, 1995.

Neretnieks, I. and A. Rasmuson, An approach to modeling radionuclide migration in a medium with strongly varying velocity and block sizes along the flow path, *Water Resour. Res.*, *20* (12), 1823-1836, 1984.

Novakowski, K.S., G.V. Evans, D.A. Lever, and K.G. Raven, A field example of measuring hydrodynamic dispersion in a single fracture, *Water Resour. Res.*, *21* (8), 1165-1174, 1985.

Sánchez-Vila, X. and J. Carrera, Directional effects on convergent flow tracer tests, *Math. Geol.*, *29* (4), 551-569, 1997.

Tsang, Y.W., Study of alternative tracer tests in characterizing transport in fractured rocks, *Geophys. Res. Letters*, 22 (11), 1421-1424, 1995.

Wagner, B.J. and J.W. Harvey, Experimental design for estimating parameters of rate-limited mass transfer: Analysis of stream tracer studies, *Water Resour. Res.*, *33* (7), 1731-1741, 1997

Welty, C. and L.W. Gelhar, Evaluation of longitudinal dispersivity from nonuniform flow tracer tests, *J. Hydrol., 153* (), 71-102, 1994.

Zlotnik, V.A. and J.D. Logan, Boundary conditions for convergent radial tracer tests and effect of well bore mixing volume, *Water Resour. Res.*, *32* (7), 2323-2328, 1996.

Figure Captions

Figure 1. Schematic diagram of polar coordinate transformation from coordinates with respect to the injection well to coordinates with respect to the pumping well.

Figure 2. Observed breakthrough curve data and the limits of the 95 percent confidence intervals for the two H-11b3 to b1 tracer tests.

Figure 3. Observed breakthrough curve data and the limits of the 95 percent confidence intervals for the two H-19b7 to b0 tracer tests.

Figure 4. Normalized sensitivities of the BTC model to each of the four estimated parameters. Sensitivities from the H-11 low test are shown as an example.

Figure 5. Multirate diffusion transport model fits to the H-11 data for both pumping rates.

Figure 6. Multirate diffusion transport model fits to the H-19 data for both pumping rates.

Figure 7. Cumulative distributions of diffusion rate coefficients as estimated from the four two-well tests. The regions of each for which the Damkohler number is between 100 (right-hand side) and 0.01 (left-hand side) are indicated.

Figure 8. Single-rate model fit to the H-11 low data. The multirate model fit is shown for comparison.

Figure 9. Single-rate model fit to the H-19 low data. The multirate model fit is shown for comparison.

Figure 10. Model fits to the H-11 high tracer test data using both multirate and single-rate models estimated on the H-11 low tracer test data.

Figure 11. Model fits to the H-19 high tracer test data using both multirate and single-rate models estimated on the H-19 low tracer test data.

Table 1: Fixed parameters for TWCF tracer tests

Parameter	H-11 "low"	H-11 "high"	H-19 "high"	H-19 "low"
Number of Data (benzoic acids)	107	75	77	67
Pumping Rate (m^3/s)	$2.23x10^{-4}$	$3.76x10^{-4}$	$2.74x10^{-4}$	$1.57x10^{-4}$
Tracer Injection Time (s)	1974	1998	960	1698
Tracer Injection Rate (m^3/s)	$9.57x10^{-5}$	$9.5x10^{-5}$	$2.06x10^{-4}$	$1.17x10^{-4}$
Chaser Injection Time (secs)	3810	3840	780	1410
Chaser Injection Rate (m^3/s)	$9.76x10^{-5}$	$9.71x10^{-5}$	$2.16x10^{-4}$	$1.19x10^{-4}$
Diffusive Porosity	0.16	0.16	0.147	0.147
Tortuosity	0.11	0.11	0.09	0.09
Aquifer Thickness (m)	4.4	4.4	4.4	4.4
Aqueous Diffusion Coefficient (m^2/s) (benzoic acids)	$7.9x10^{-10}$	$8.2x10^{-10}$	$8.2x10^{-10}$	$8.0x10^{-10}$
Distance Between Wells (m)	20.9	20.9	12.2	12.2

Table 2: Multirate parameter estimation results for TWCF tracer tests.

Test	$\mu_d \pm 2\sigma$ range	σ_d $ln(\sigma_d \pm 2\sigma)$ range	ϕ_a $ln(\phi_a \pm 2\sigma)$ range	$\alpha_L(m)$ $ln(\alpha_l \pm 2\sigma)$ range	RMSE
H-11 Low n = 107	-17.7 ± 0.9 -18.6, -16.8	1.3 0.3 ± 0.7 0.7, 2.6	1.3×10^{-3} -6.6 ± 0.8 6.1×10^{-4}, 2.8×10^{-3}	3.4 1.2 ± 0.3 2.5, 4.5	0.09
H-11 High n = 75	-17.2 ± 1.3 -18.5, -15.9	1.1 0.1 ± 0.2 0.9, 1.4	6.2×10^{-4} -7.4 ± 0.6 3.4×10^{-4}, 1.0×10^{-3}	3.0 1.1 ± 2.6 0.2, 39.3	0.12
H-19 Low n = 67	-16.2 ± 0.6 -16.8,-15.6	5.5 1.7 ± 3.5 0.2, 180.2	3.7×10^{-3} -5.6 ± 0.2 2.6×10^{-3}, 5.7×10^{-3}	1.0 0.0 ± 0.9 0.4, 2.4	0.12
H-19 High n = 77	-15.2 ± 0.9 -16.1, -14.2	5.5 1.7 ± 2.5 0.4, 68.9	8.5×10^{-4} -7.1 ± 0.02 8.3×10^{-4}, 8.6×10^{-4}	1.1 9.5×10^{-2} ± 0.7 0.5,2.2	0.13

Table 3: Values of parameters estimated using a single-rate TWCF model

Test	μ_d	σ_d	ϕ_a	α_L (m)	ϕ_d	RMSE
H-11 Low n=107	-19.5	0.0	8.2×10^{-04}	2.44	0.16	0.18
H-19 Low n=67	-21.1	0.0	5.7×10^{-02}	2.4	0.094	0.16

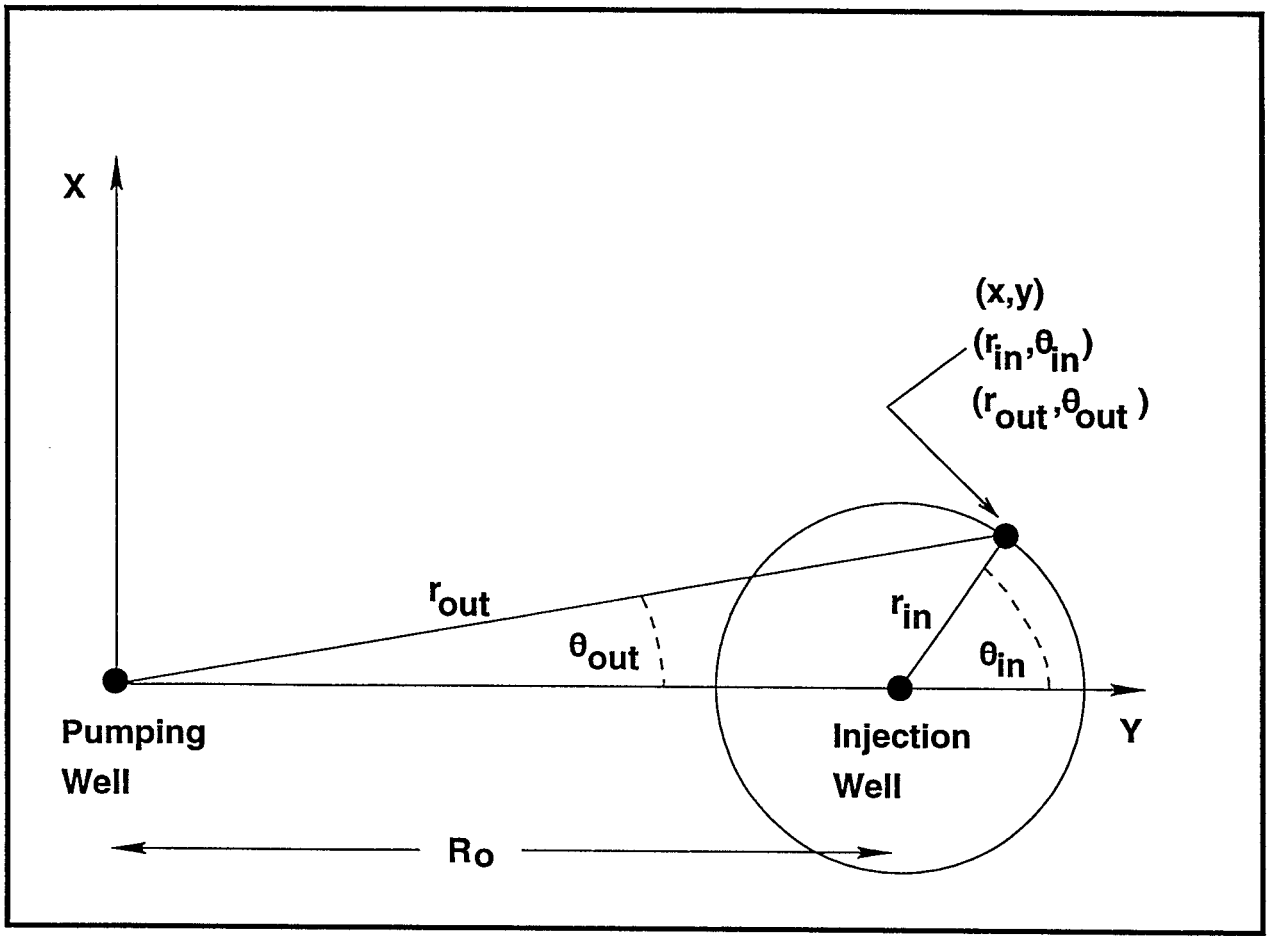
X
(x,y)
(r_in,θ_in)
(r_out,θ_out)
r_out
θ_out
r_in
θ_in
Pumping
Well
Injection
Well
Y
Ro

Fig. 1

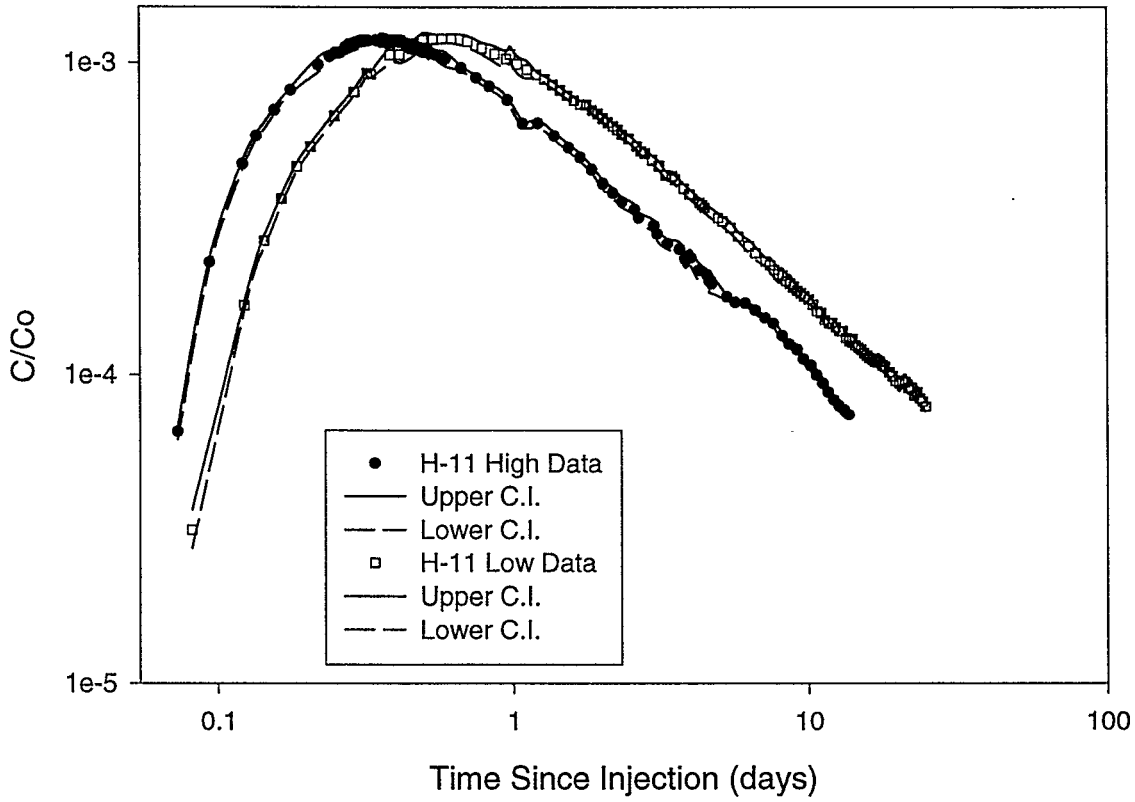
1e-3
1e-4
1e-5
C/Co
0.1
1
10
100
Time Since Injection (days)
H-11 High Data
Upper C.I.
Lower C.I.
H-11 Low Data
Upper C.I.
Lower C.I.

Fig 2

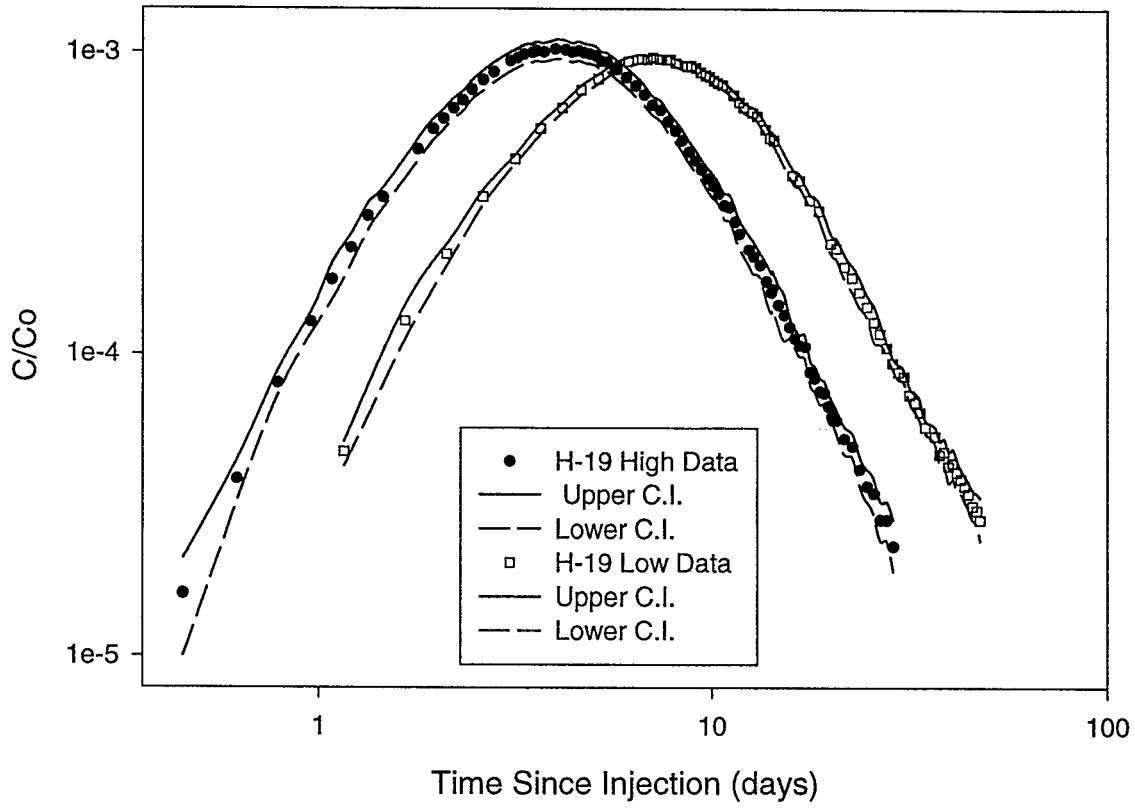
1e-3
1e-4
1e-5
C/Co
1
10
100
Time Since Injection (days)
H-19 High Data
Upper C.I.
Lower C.I.
H-19 Low Data
Upper C.I.
Lower C.I.

Fig 3

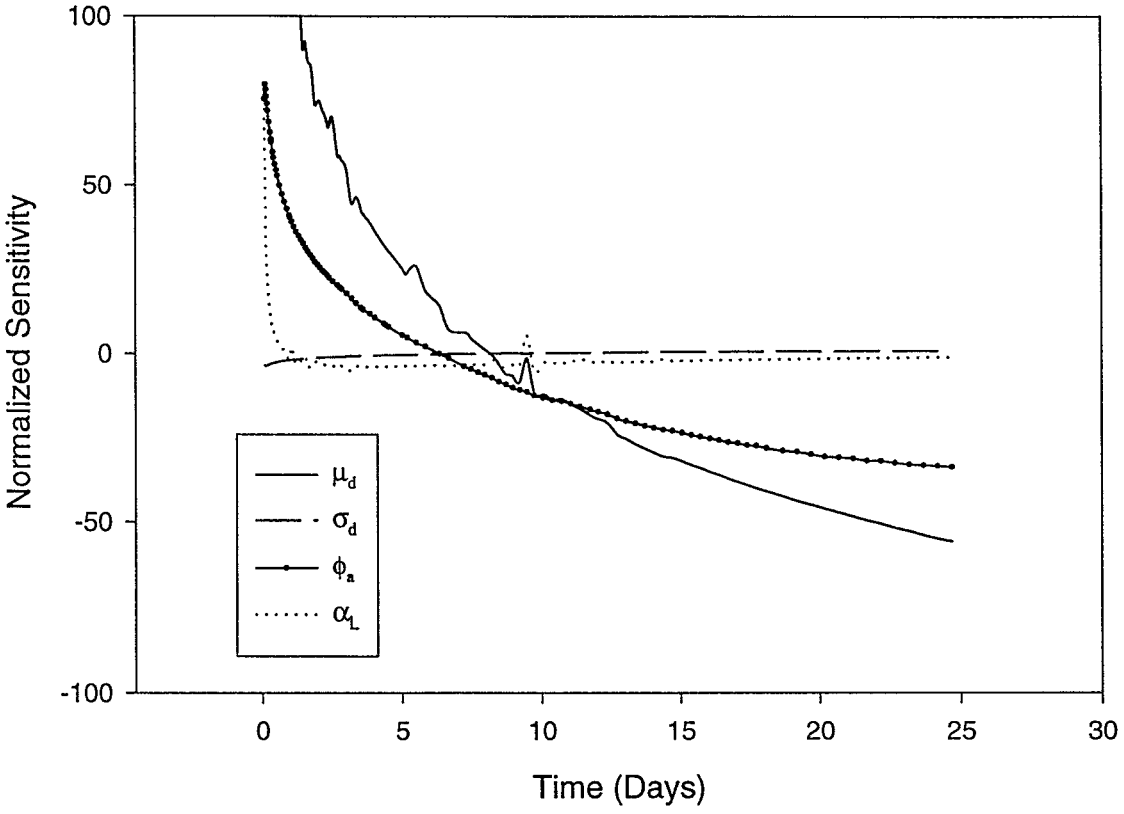
100
50
0
-50
-100
Normalized Sensitivity
0
5
10
15
20
25
30
Time (Days)
μ_d
σ_d
ϕ_a
α_L

Fig 4

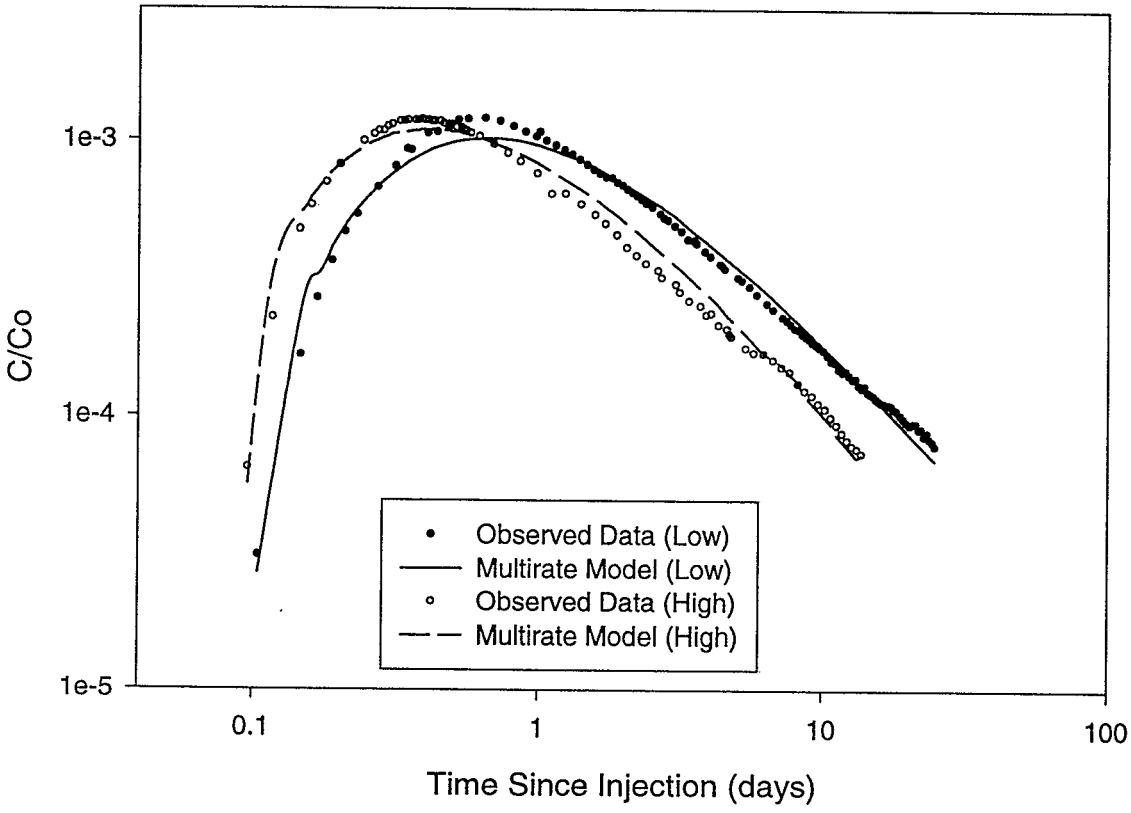
1e-3
1e-4
1e-5
C/Co
0.1
1
10
100
Time Since Injection (days)
Observed Data (Low)
Multirate Model (Low)
Observed Data (High)
Multirate Model (High)

Fig 5

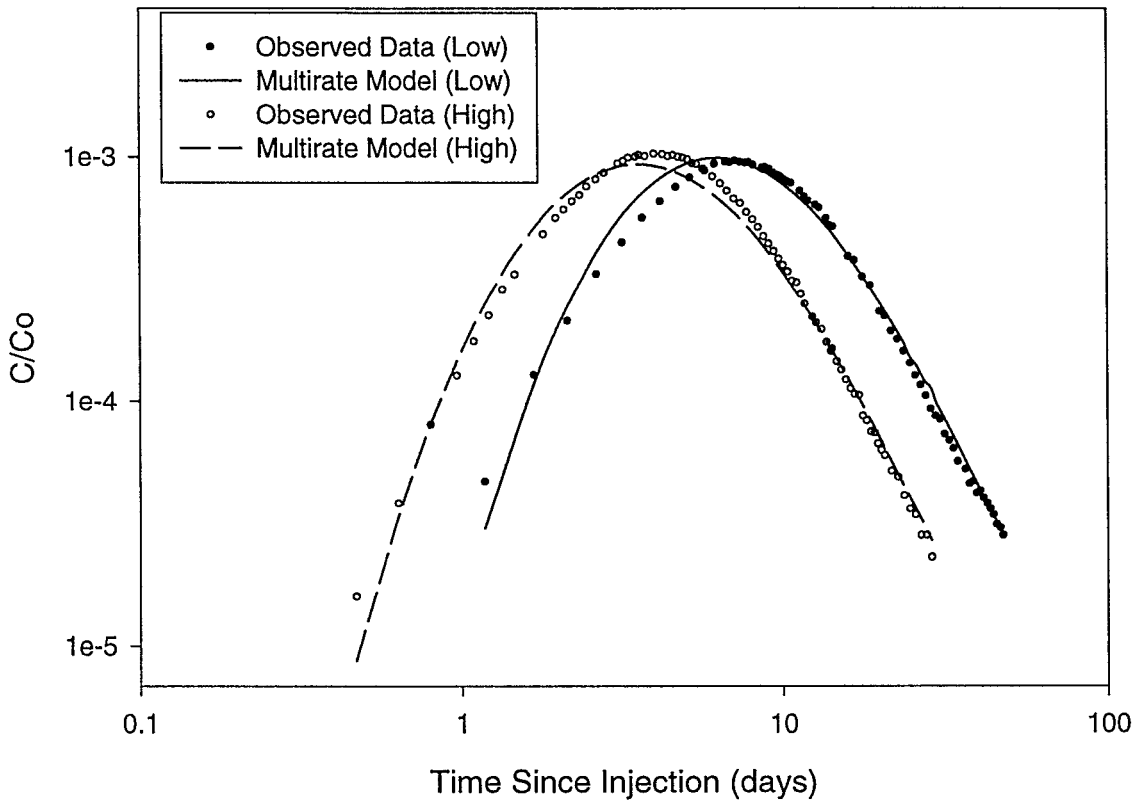
Observed Data (Low)
Multirate Model (Low)
Observed Data (High)
Multirate Model (High)
1e-3
1e-4
1e-5
C/Co
0.1
1
10
100
Time Since Injection (days)

Fig 6

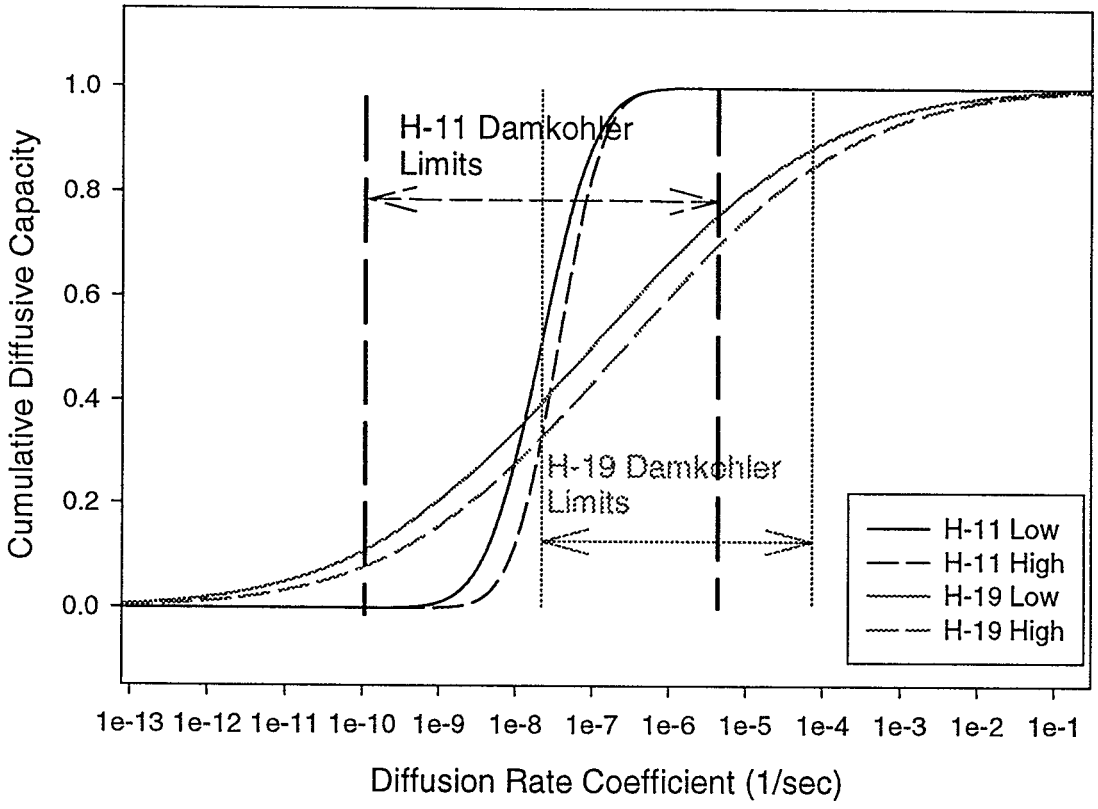
Cumulative Diffusive Capacity
1.0
0.8
0.6
0.4
0.2
0.0
H-11 Damkohler Limits
H-19 Damkohler Limits
H-11 Low
H-11 High
H-19 Low
H-19 High
1e-13 1e-12 1e-11 1e-10 1e-9 1e-8 1e-7 1e-6 1e-5 1e-4 1e-3 1e-2 1e-1
Diffusion Rate Coefficient (1/sec)

Fig 7

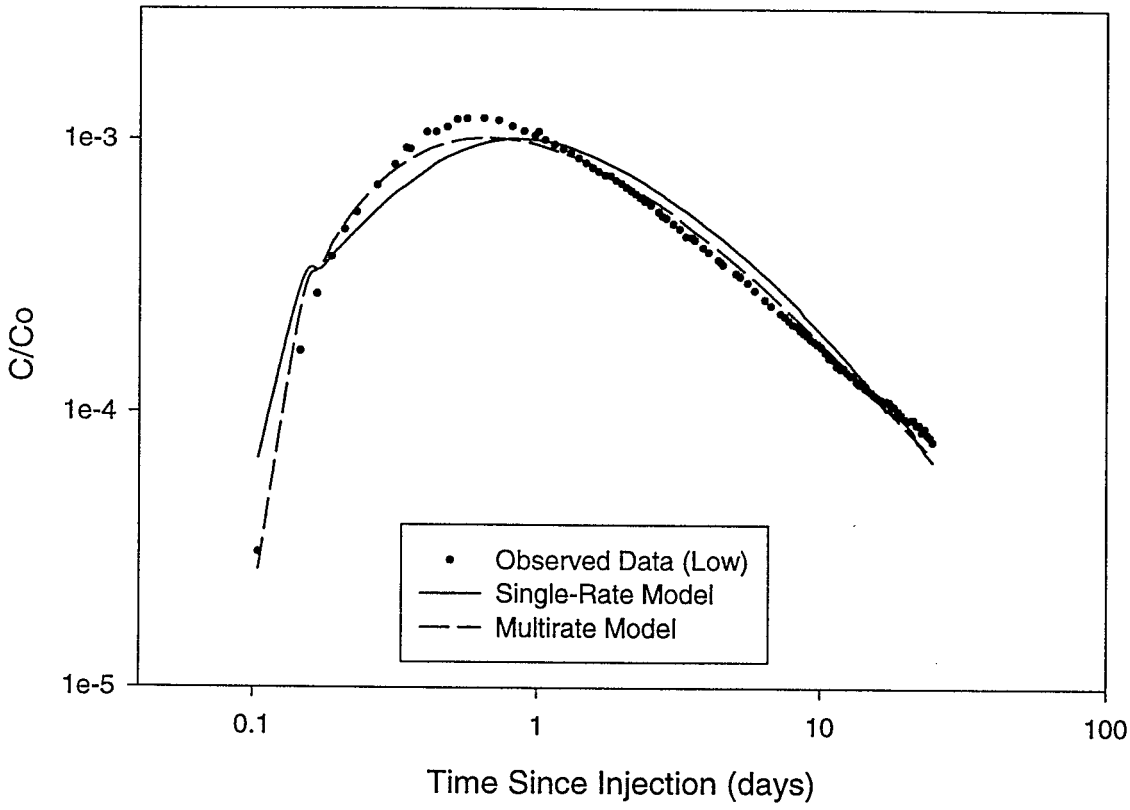
1e-3
1e-4
1e-5
C/Co
0.1
1
10
100
Time Since Injection (days)
Observed Data (Low)
Single-Rate Model
Multirate Model

Fig 8

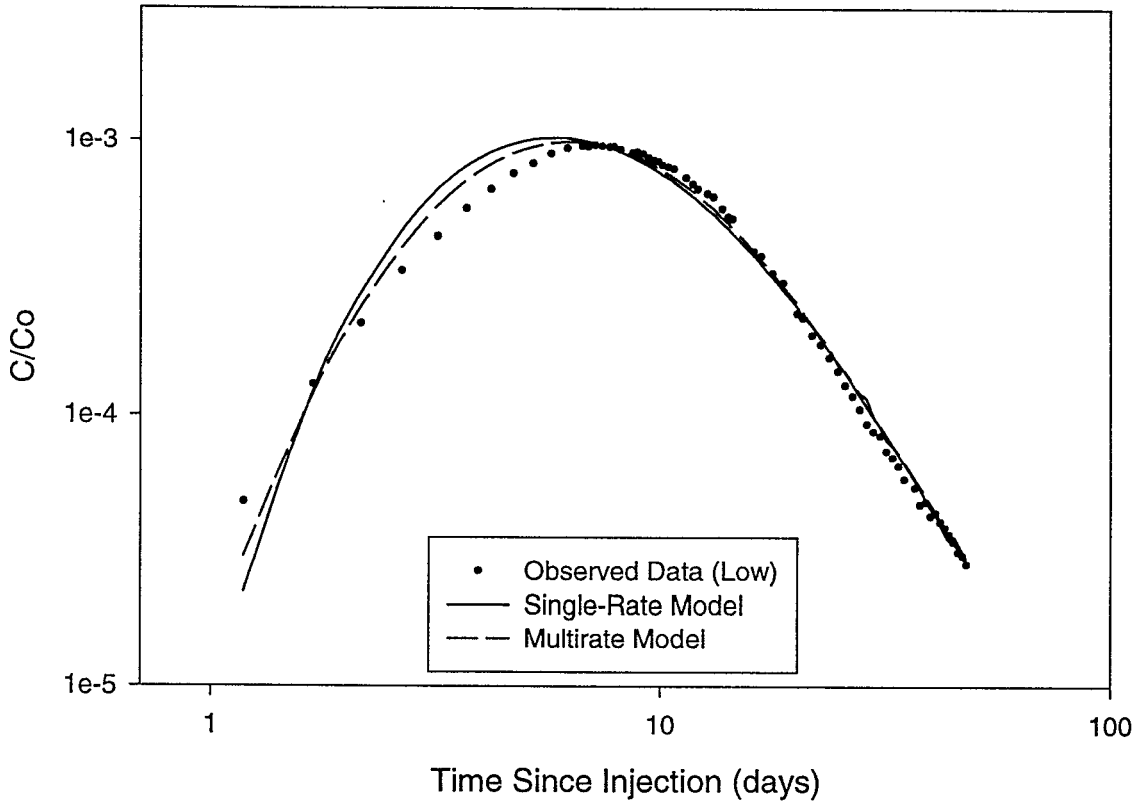
1e-3
1e-4
1e-5
C/Co
1
10
100
Time Since Injection (days)
Observed Data (Low)
Single-Rate Model
Multirate Model

Fig 9

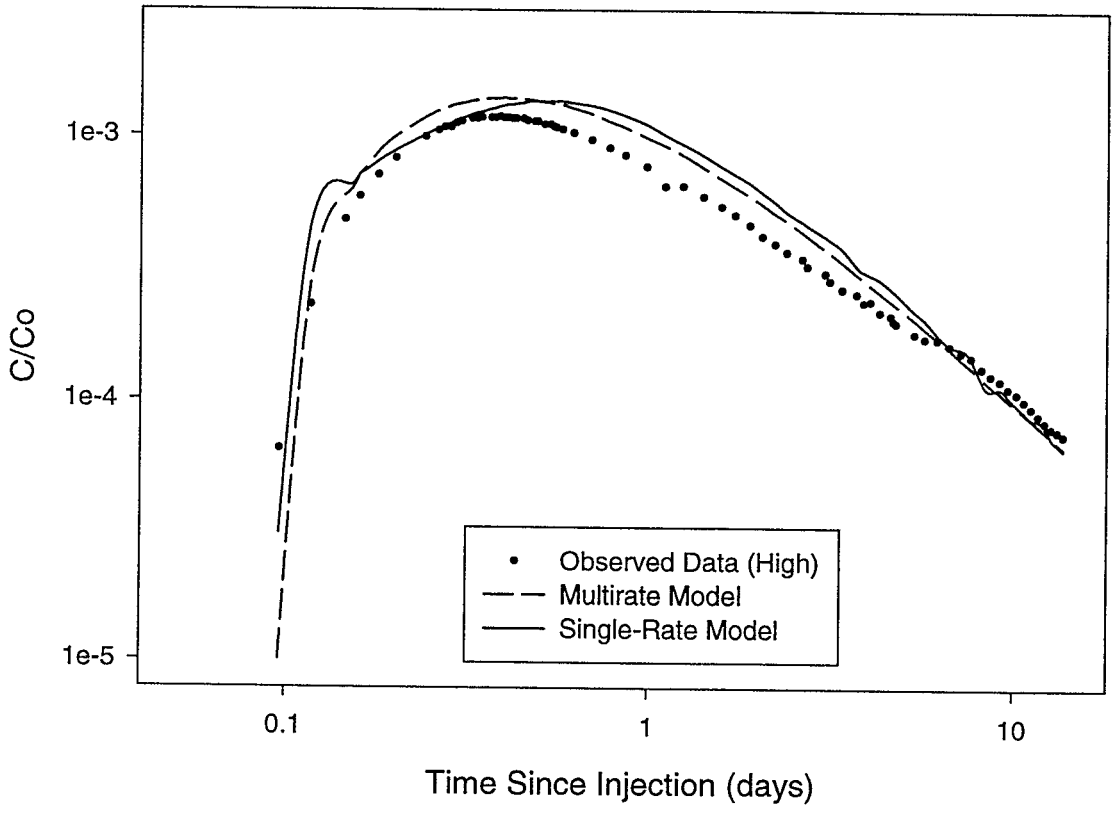
1e-3
1e-4
1e-5
C/Co
0.1
1
10
Time Since Injection (days)
Observed Data (High)
Multirate Model
Single-Rate Model

Fig 10

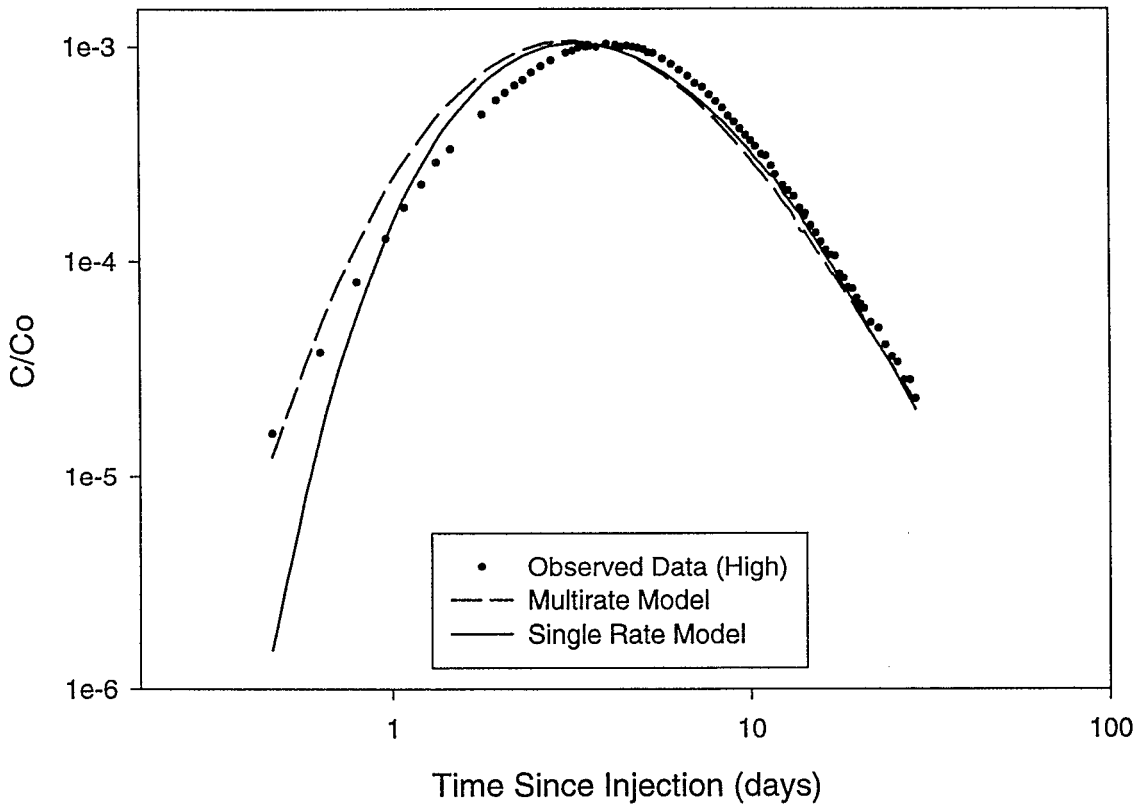
1e-3
1e-4
1e-5
1e-6
C/Co
1
10
100
Time Since Injection (days)
Observed Data (High)
Multirate Model
Single Rate Model

Fig 11